AUT Journal of Electrical Engineering

AUT J. Elec. Eng., 54(special issue 2) (2022) 333-342
DOI: 10.22060/eej.2022.21376.5471

Optical Sensors for Industrial and Biomedical Applications

A. Mataji-Kojouri[1], A. Nooramin[2], M. Shahabadi[1]*

[1] Photonics Research Lab., School of Electrical and Computer Engineering, College of Engineering University of Tehran, Tehran, Iran
[2] School of Electrical Engineering, Iran University of Science and Technology, Tehran, Iran

ABSTRACT: This article begins with a brief review of those industrial and biomedical optical sensors which have been designed and fabricated in Photonics Research Laboratory at the University of Tehran. Firstly, development of a fiber-based fluid temperature and pressure sensing system is described. Afterwards, a frequency-modulation interferometric sensor enabling low-cost and highly sensitive refractive index measurement is presented. Having introduced these categories of sensors, we briefly describe the Transmission-Line Formulation (TLF) method which has been developed for the diffraction analysis of optical periodic structures. The application of this method is demonstrated to the design of a coupled cross-stacked Guided-Mode Resonance sensor with a high surface sensitivity. We further review the design of dual-resonance nanostructured plasmonic sensors that can be used to differentiate background refractive index variation from adsorption of a layer on the sensing surface, and to estimate the thickness of adsorbed layers. Finally, we use the TLF method to design a spectrometer-free configuration for a dual-mode plasmonic sensor, which substantially simplifies the measurement setup.

Review History:
Received: May, 06, 2022
Revised: Jun. 30, 2022
Accepted: Jul. 02, 2022
Available Online: Dec. 01, 2022

Keywords:
Optical fiber sensors
interferometric optical sensors
refractive index sensors
plasmonic sensing
plasmonic ruler

1- Introduction

Optical sensors are increasingly used in industries that other types of sensors like electric sensors are not desirable. To avoid electric sensors, one can alternatively employ optical sensors, which can be connected to their sensing systems by optical signals. With the help of optical fibers, these signals can travel long distances without a considerable loss, making measurement at remote distances possible. Fiber-based optical sensors offer great advantages over other sensing technologies in harsh environments where immunity to electromagnetic interference is required, and electric discharges must be avoided. These sensors are also highly resistant to corrosion and tolerate high temperatures and pressures. Moreover, optical sensors provide unprecedented sensitivity in detection of trace concentrations of analytes in a sample, lending themselves to various industrial and biomedical applications [1]–[3].

In this paper, we focus on our efforts toward design and implementation of different optical sensors at the Photonics Research Lab., School of Electrical and Computer Engineering, University of Tehran. These sensors include fiber-based temperature and pressure sensors, free-space interferometric sensors [4], and sensors with periodic structures [5]–[7]. In Section 2, we report on our fiber-based fluid temperature and pressure sensors and present their specifications. In Section 3, we describe an interferometric refractive index sensor based on frequency modulation of a laser diode which can be readily adapted for portable measurements [4]. In Section 4, we focus on sensors with periodic structures. First a numerical method for the analysis of periodic structures is shortly described [8]. Afterwards, we discuss a Guided-Mode Resonance (GMR) sensor with a high surface-sensitivity and another plasmonic sensor, which can differentiate bulk refractive-index variations from formation of a layer on top of the sensing surface. Hereafter, we outline the results of a dual-resonance nanoplasmonic sensor that can measure the thickness of the layers adsorbed on its surface. Next, we propose a spectrometer-free configuration for performing measurements on the dual-resonance plasmonic sensor. We finally conclude the paper in Section 5.

2- Fiber-optic-based Fluid Temperature/Pressure Sensor

In our first attempt, we focused on Fabry-Perot-based sensors for measuring temperature and pressure of a fluid due to their high compatibility with optical fibers [9]. Fig. 1a shows a Fabry-Perot resonator composed of two optical fibers that are mounted inside a capillary tube. Fig. 1b shows a schematic of a similar sensor where one of the fibers is coated with a thin gold layer in order to achieve higher back reflection. As shown in the figure, two optical fibers are positioned with a gap of length inside a capillary tube. To fabricate the sensor, first a cleaved-cut fiber is coated with

*Corresponding author's email: shahabad@ut.ac.ir

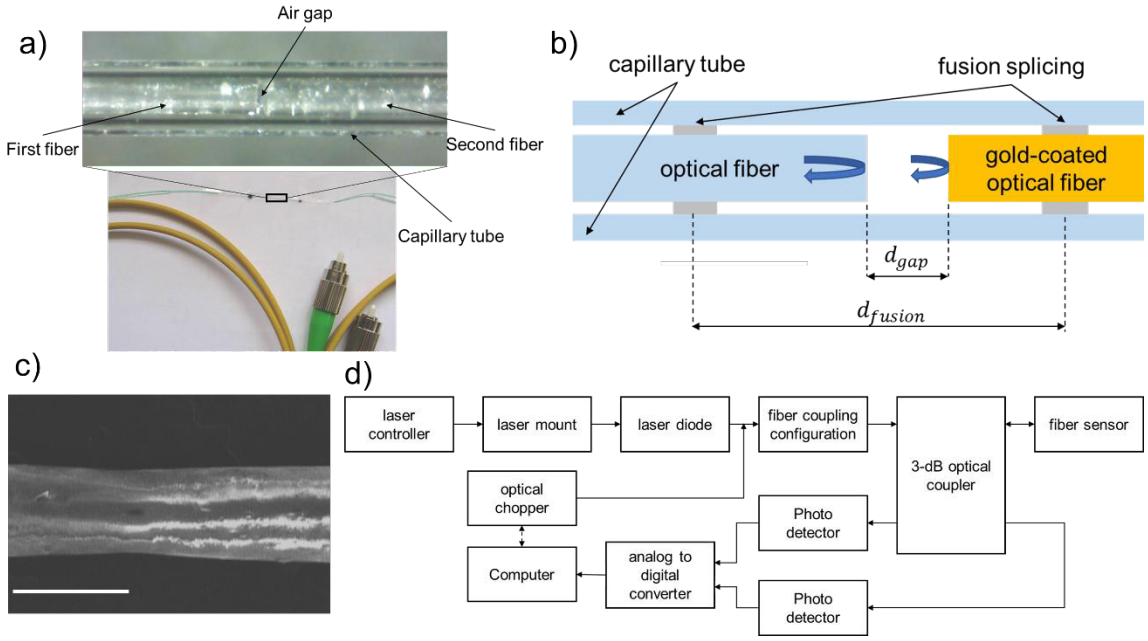

Fig. 1. a) The fabricated optical sensor (bottom panel) and a magnified view of the Fabry-Perot resonator formed between two optical fibers inside a capillary tube (top panel). b) A schematic of the Fabry-Perot-based optical-fiber sensor, composed of an input-output optical fiber on the left, and another gold-coated fiber acting as a reflector. The fibers are connected to a capillary tube using CO2-laser welding. Any variation in the length of the capillary tube due to temperature or pressure will change the length of the Fabry-Perot resonator d_{gap} and can be monitored through the input-output optical fiber. c) SEM image of an optical fiber connected to the capillary tube using laser welding. The scale bar is 300 µm. d) Block diagram of the measurement setup. Light emitted from a laser diode is coupled to an optical fiber after passing through an optical chopper. A 3-dB optical coupler excites the sensor and delivers the reflected light to the first photodetector. It also delivers parts of the input light directly to the second photo-detector. Outputs of the photodetectors are then converted to digital signals and analyzed by a computer.

gold to form a mirror. This fiber is attached to one end of the capillary tube by CO2-laser welding. A second cleaved-cut fiber, which is also welded to the capillary tube, excites the resonator. In addition, the discontinuity at the end face of this fiber provides the second reflection required for forming a Fabry-Perot resonator. Fig. 1c shows a Scanning Electron Microscope (SEM) image of the optical fiber installed in the capillary tube. By selecting the proper material and structure for the capillary tube, one can transduce variations in either pressure or temperature of the fluid to changes in the length of the capillary tube. This will in turn change the length of the Fabry-Perot resonator (d_{gap}), which can be monitored in real-time by analyzing the reflected optical signal from the sensor. Fig. 1d shows a block diagram of the measurement setup. Output of a Multi-Quantum-Well (MQW) laser at a wavelength of 1550 nm is coupled into the input optical fiber and excites the sensor after passing through an optical coupler. The coupler then delivers the reflected signal from the sensor to a photodetector. To increase the range of the detectable signals, the input laser signal is modulated by an optical chopper and a lock-in amplifier is implemented in data analysis algorithm. The sensor provides an error smaller than 0.5 bar for pressures between 15 to 40 bar, and an absolute error of 0.5 degrees of Celsius for temperatures between to .

3- Refractive Index Measurement based on Deep Frequency Modulation Interferometry

Optical interferometry is a widely-used technique for high-resolution RI sensing [10]. However, it usually needs complex optical setups and expensive optical devices, such as optical modulators. Here, we focus on deep frequency-modulation interferometry [11]–[15]. The modulation index in this method is one order of magnitude larger than that the conventional frequency modulation, and a greater number of harmonics is used to extract the optical path length difference between the interferometer arms. We have presented a low-cost implementation of this interferometry, which enables highly sensitive refractive index measurement [4]. Fig. 2a shows a schematic of our interferometer. In this implementation, frequency modulation is realized by modulating the amplitude of the driving current of a laser diode. This technique substantially reduces the complexity of the optical setup compared to the configurations, based on optical modulators. Fig. 2b shows the driving current of the laser diode and the output signals of the photodetector for two different fluids. After careful analysis of the collected photodetector signals, it is possible to extract the path-length difference between the arms of the interferometer caused by RI variation of the fluid under test [4]. Fig. 2c shows

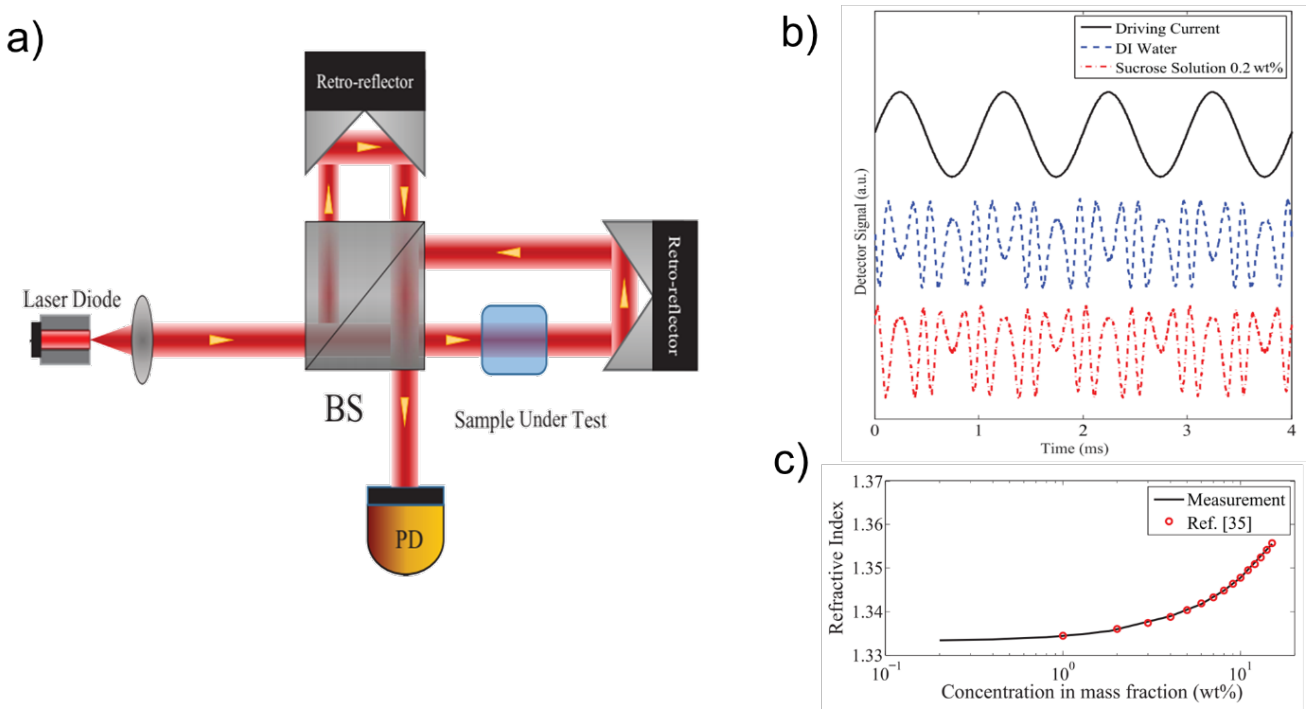

Fig. 2. a) A schematic of the measurement setup used for optical interferometry (BS: beam splitter, PD: photodetector). b) Laser diode drive signal and photodetector output signals for DI water and sucrose solution. c) Measured and reference values for refractive indices of sucrose solutions with different mass concentrations. Reprinted with permission from [4].

the measured values for the refractive indices of sucrose solutions with different concentrations. Our results are in agreement with previously reported data for these solutions. The proposed interferometer provides high-precision and real-time measurement of RI with a resolution higher than 2.1 × 10−5 Refractive Index Unit (RIU).

4- Periodic Optical Biosensors

In this section, we first describe the Transmission-Line Formulation method that is developed for the numerical analysis of optical diffraction by periodic structures. Thereafter, we focus on our periodic nanostructured sensors which are either based on Guided-Mode Resonance or Surface Plasmon resonance phenomena [5]–[7].

4- 1- Transmission Line Formulation for the Analysis of Periodic Structures

Fig. 3 shows a four-layer periodic structure illuminated by a TE-polarized plane wave. The relative permittivity function in the periodic layer is defined by $\varepsilon_r(x)$, and the periodicity of the structure is L. Therefore, the permittivity function can be represented by a Fourier series as:

$$\epsilon_r(x) = \lim_{N\to\infty} \sum_{n=-N}^{N} \tilde{\epsilon}_n e^{-\frac{j2n\pi x}{L}} \quad (1)$$

For this configuration, according to the Bloch-Floquet theorem, the tangential components of the electric and magnetic fields can be described by:

$$E_z(x,y) = \lim_{N\to\infty} \sum_{n=-N}^{N} E_{Zn}(y) e^{-j\alpha_n x}, \quad (2)$$

$$H_x(x,y) = \lim_{N\to\infty} \sum_{n=-N}^{N} H_{Xn}(y) e^{-j\alpha_n x}, \quad (3)$$

where $\alpha_n = k_x + 2n\pi x / L$, and k_x stands for the x-component of the wave-vector of the incident plane wave. By substituting (1)-(3) in Maxwell's equations, a matrix

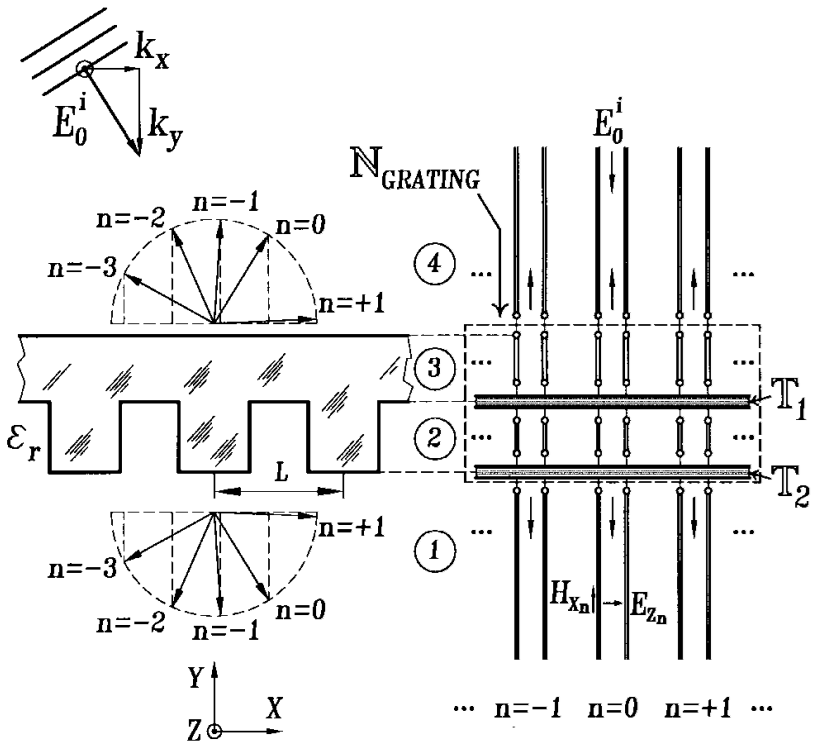

Fig. 3. A four-layer periodic structure illuminated with a TE-polarized plane wave and its equivalent network model. Reprinted with permission from [8].

relation governing the unknown coefficients of (2) and (3) is obtained, which is similar to the equations of the telegrapher for multi-conductor transmission lines. By truncating the above Fourier expansions and applying boundary conditions at the interface of successive layers as described in [8], one can calculate the solution to the scattering problem and determine the optical diffraction properties of the periodic structure under investigation. A similar procedure can be followed to analyze biperiodic structures [16], anisotropic waveguides [17], [18], and other periodic structures [19]–[23].

4- 2- GMR Sensor with Enhanced Surface Sensitivity Using Coupled Cross-Stacked Gratings

Guided-Mode Resonance is a phenomenon that can be observed in periodic dielectric structures, such as waveguide-gratings and photonic-crystal slabs that support leaky waves. The GMR occurs when the phase match condition between the complex propagation constant of the leaky wave and one of the diffraction orders of the periodic structure are satisfied. Resonances of these structures are highly sensitive to any changes of RI of the medium adjacent to the structure [24]–[26]. Most of the studies on GMR sensors focus on their high bulk sensitivity, and minor attention has been paid to biosensors with large surface sensitivity. Hence, we designed a GMR sensor based on coupled gratings with high energy density localization near the waveguide-grating. This yielded a high sensitivity to the variations of RI near the sensor surface. Fig. 4a shows a schematic of the unit cell of the proposed GMR sensor. Fig. 4b shows the reflection spectrum of a typical coupled cross-stacked GMR structure with $d_w = 400\ nm$, $d_g = 100\ nm$, $ff_w = 0.5$, $ff_g = 0.5$, $\Lambda = 1000\ nm$. In our analysis, $n_{SiO_2} = 1.46$, and $n_{SiN_x} = 2$, and the refractive index of the water surrounding the sensor is assumed to be n_{H_2O} =1.33 at the operating wavelength. Fig. 4c and Fig. 4d show magnitude of the y-component of the electric field for TE polarized incident light at resonance wavelengths of λ = 1554.645 nm and λ = 1624.652 nm, respectively. It can be seen that the field enhancement of more than 100 is possible using the proposed sensor. We also studied impact of different parameters of the structure on the performance of the sensor. Based on our calculations, a sensor with $d_w = 325\ nm$, $d_g = 50\ nm$, $ff_w = 0.5$, $ff_g = 0.25$, $\Lambda = 1000\ nm$ provides a surface sensitivity twice the conventional GMR sensors, and its quality factor is higher than 70000.

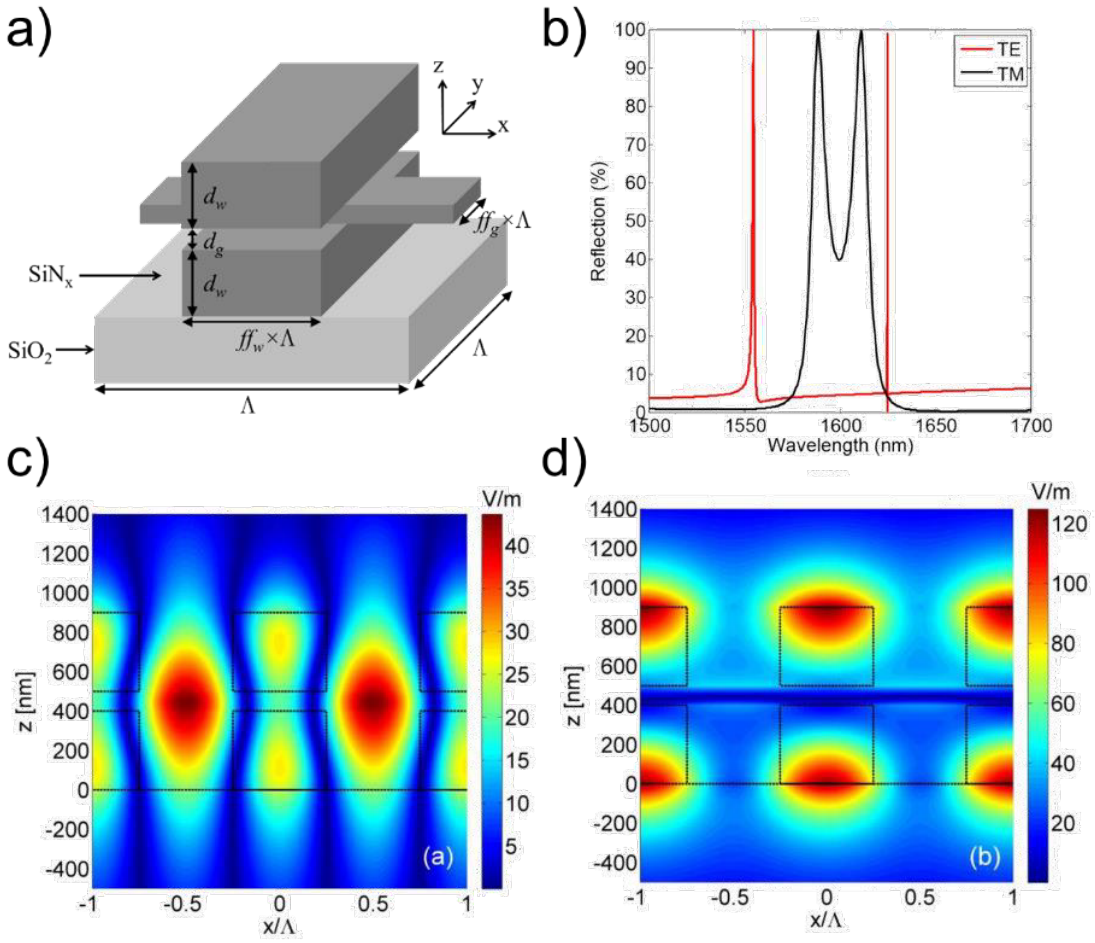

Fig. 4. a) Unit cell of the coupled cross-stacked GMR sensor. b) Reflection spectrum for normal incident light for both TE and TM polarizations. Magnitude of y-component of electric field for TE-polarized incident light at resonance wavelengths of (c) λ=1554.645 nm, and (d) λ=1624.652 nm. The borders of the waveguide-gratings and the substrate are drawn by dotted lines. Reprinted with permission from [5].

4- 3- Plasmonic Biosensors for Estimating the Thickness of the Surface Adsorbed Analytes

Plasmonic biosensors are proposed for applications in point-of-care and real-time clinical evaluation and disease diagnosis [27]. However, it is not immediately distinguishable whether a signal shift is due to a binding event or unwanted RI variations in the background solution. Dual resonance plasmonic sensors can overcome this limitation [28]–[30]. Previously, we reported a hybrid photonic-plasmonic sensor composed of an array of nanogrooves for differentiating surface and background RI variations [6]. In this sensor, the photonic mode is mainly sensitive to bulk RI variations, thanks to its field distribution in the bulk solution. The plasmonic mode of this structure is tightly localized inside the nanogrooves of the structure. Hence, it is mostly sensitive to adsorption of analytes on the sensor surface. By monitoring the resonances of this structure simultaneously, one can distinguish bulk RI variations from surface binding events.

Estimating thickness of the adsorbed layer on the sensing surface may be of clinical interest in various cases [7]. Optical sensors can be used to estimate the thickness of adsorbed layers [31]–[33]. We recently reported a dual-mode plasmonic sensor that both eliminates background RI variations and provides thickness of the surface-adsorbed layers [7]. The structure is a 1D gold grating with a periodicity of $1.1\ \mu m$. The corrugation width is 650 nm and its height is 35 nm. Fabrication of this sensor is straightforward and its measurement setup employs a portable spectrometer, which reduces the costs of the sensing system. Fig. 5a shows a picture of the fabricated sensor and a SEM image of its cross-section. Once the structure is illuminated by a normal plane wave with TM polarization, its reflection spectrum shows two resonances (Fig. 5b). Fig. 5c shows the electric field lines and field distribution at these two resonances. The first resonance which has a rapidly decaying field distribution resembles a Localized Plasmon (LP) resonance. The second resonance is

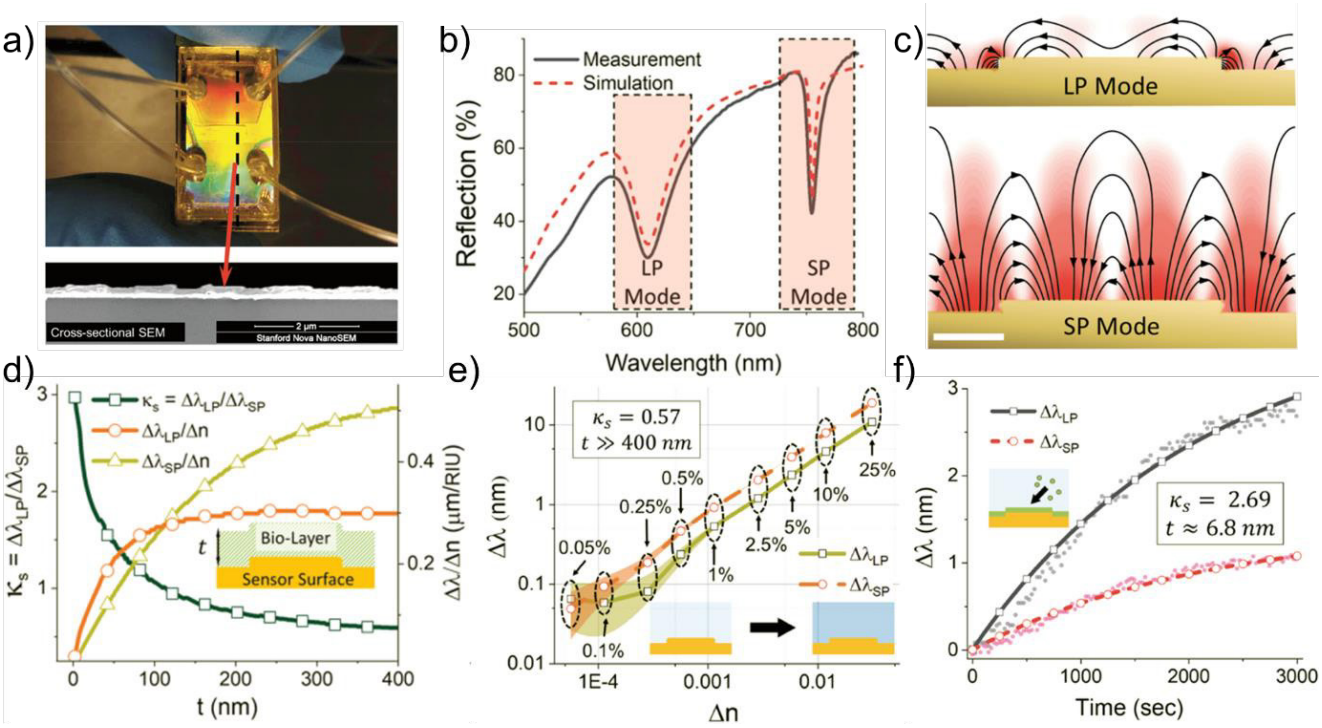

Fig. 5. a) A picture of the sensor and the fabricated microfluidic channel (top panel), and SEM image of the fabricated sensor (bottom panel). b) Simulated and measured reflection spectra of the sensor. c) Electric field magnitude and electric field lines for the LP and SP resonances. Scale bar is 200 nm. d) normalized wavelength shifts of the LP and SP resonances (right axis) and their ratio $\kappa_s=\Delta\lambda_{LP}/\Delta\lambda_{SP}$ (left axis) calculated for adsorbed layers with different thicknesses (t). In this calculation, RI of the adsorbed layer is n = 1.38 (Δn = 0.05), and the shift values are normalized to Δn=0.05. Reprinted with permission from [7]. Copyright (2020) American Chemical Society.

similar to a propagating Surface Plasmon (SP) resonance and its decay length is substantially larger than the LP resonance. Fig. 5d shows the LP and SP resonance wavelengths shifts, and their ratio once an adsorbed layer forms on the sensing surface. As shown in this figure, the LP resonance shifts more than the SP resonance for thin layers (a few tens of nanometer). However, the SP resonance shifts more once the adsorbed layer is thicker. Our calculations show that the ratio of the resonance shifts $\kappa_s = \Delta\lambda_{LP} / \Delta\lambda_{SP}$ does not depend on the refractive index of the adsorbed layer, but mostly on its thickness. Fig. 5e shows measured resonance shift values for aqueous glycerol solutions with different concentrations. The ratio of wavelength shifts for this experiment amounts to $\kappa_S = 0.57$ which is in agreement with our calculations for background RI variation. Fig. 5f shows the resonance shift values during binding of NeutrAvidin on the sensor surface. In this experiment, the value of κ_S is 2.69. Based on Fig. 4d, this ratio corresponds to formation of a 6.8 nm-thick layer. We further estimated the thickness of a layer composed of exosomes formed on the sensing surface [7]. These results suggest that the sensor can be used to study concentration and size of biological nanoparticles.

4- 4- Spectrometer-free Configuration for Dual Resonance Sensing

Here, we investigate the response of the dual-resonance plasmonic sensor under oblique incidence as a first step in developing a spectrometer-free measurement setup. Fig. 6a shows a minus-first-order reflection spectrum from the structure for different incident angles and different wavelengths. Based on these calculations, we select an incident angle of $\theta = 32.75°$. Fig. 6b shows the reflected diffraction spectra under this incident angle. The inset shows a schematic of the proposed measurement setup, where an array photodetector is placed at a distance of 15 cm from the sensor to collect the reflected diffraction order. The top horizontal axis shows the magnitude of the reflected power at different positions on the photodetector. Our calculations suggest that commercially available photodetector arrays can be used to develop a low-cost dual-resonance plasmonic sensing system. Fig. 6c and Fig. 6d show the magnitude of electric field phasor and electric field lines at $\lambda_0 = 633\ nm$ and $\lambda_0 = 755\ nm$, respectively. The distinct decay rate at the two resonances suggests that under oblique incidence, it is still possible to differentiate bulk RI variations from surface binding events.

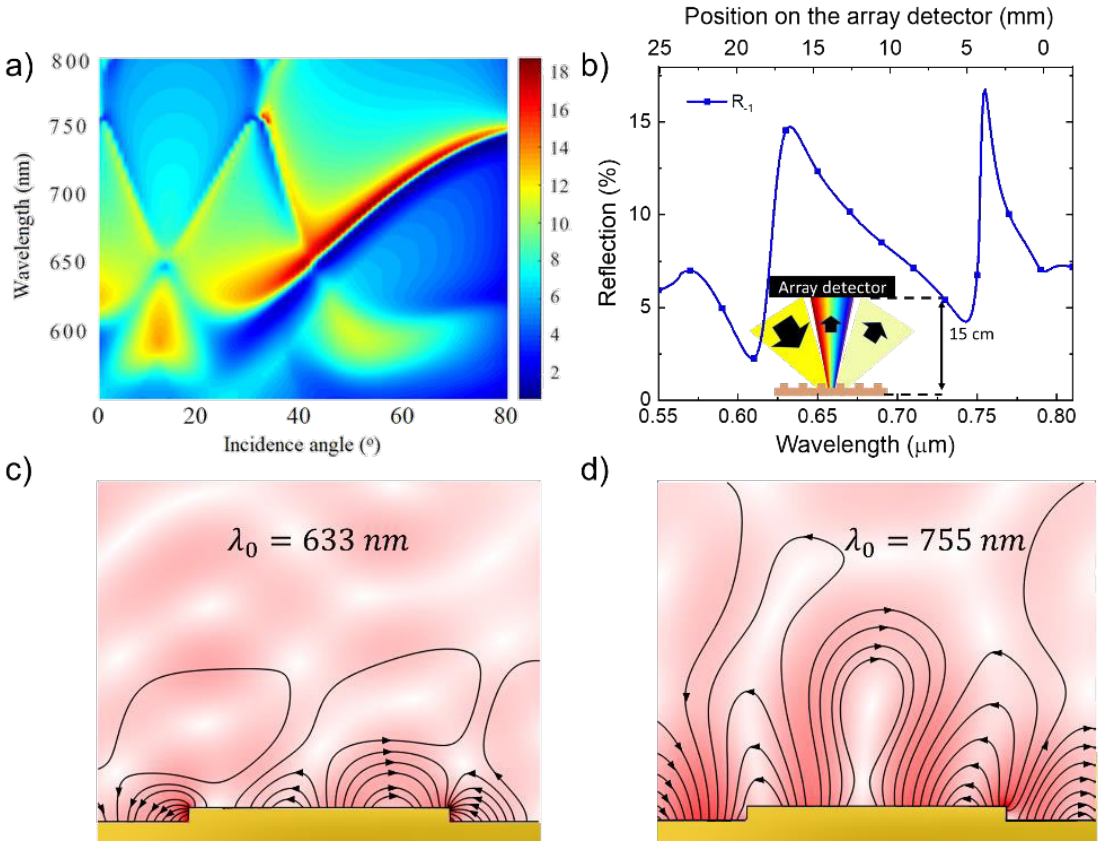

Fig. 6. a) Calculated reflected minus-first-order diffraction from the sensor for different incident angles and wavelengths. b) Calculated reflected minus-first-order diffraction for an incident angle of θ=32.75 ° for different wavelengths. The inset shows schematic of a spectrometer-free configuration for dual mode plasmonic sensing. The top axis shows the position of the diffracted light on the array photodetector for each wavelength. Magnitude of electric field phasor and electric field lines for (c) the first resonance at λ_0=633 nm and (d) λ_0=755 nm.

5- Conclusions

In this paper, we reviewed the optical sensors that we developed over the past years for different industrial and biomedical applications. It is shown that fiber-based optical sensors are suitable for remote measurements in harsh environments where immunity to electromagnetic interference is required and electric discharges must be avoided. We also showed that free-space interferometric optical sensors can offer an affordable and highly sensitive solution for portable refractive index measurements. However, to detect a specific analyte inside a complex biological solution, more complex sensors are required. In this regard, we introduced a Fourier-based computational method for the analysis of periodic structures. We then described different nanostructured biosensors that are designed using this method. We showed that surface sensitivity of a GMR sensor can be enhanced using a coupled crossed-grating structure. Afterwards, we demonstrated that dual-mode plasmonic sensors can be used to differentiate background refractive index variations from surface binding event to estimate the thickness of an adsorbed layer. Finally, we proposed a spectrometer-free configuration for dual-resonance plasmonic sensing.

References

[1] N. Khansili, G. Rattu, and P. M. Krishna, "Label-free optical biosensors for food and biological sensor applications," Sensors Actuators B Chem., vol. 265, pp. 35–49, Jul. 2018.

[2] H. E. Joe, H. Yun, S. H. Jo, M. B. G. Jun, and B. K. Min, "A review on optical fiber sensors for environmental monitoring," Int. J. Precis. Eng. Manuf. Technol. 2018 51, vol. 5, no. 1, pp. 173–191, Feb. 2018.

[3] C. Chen and J. Wang, "Optical biosensors: an exhaustive and comprehensive review," Analyst, vol. 145, no. 5, pp. 1605–1628, Mar. 2020.

[4] S. A. Akbarzadeh-Jahromi and M. Shahabadi, "Low-Cost Highly Sensitive Refractive Index Measurement Based on Deep Frequency Modulation Interferometry," IEEE Sens. J., vol. 17, no. 17, pp. 5460–5465, Sep. 2017.

[5] S. A. J. Moghaddas, M. Shahabadi, and M. Mohammad-Taheri, "Guided mode resonance sensor with enhanced surface sensitivity using coupled cross-stacked gratings," IEEE Sens. J., vol. 14, no. 4, pp. 1216–1222, Apr. 2014.

[6] H. Neshasteh, A. Mataji-Kojouri, S. A. Akbarzadeh-

Jahromi, and M. Shahabadi, "A Hybrid Photonic-Plasmonic Sensing Platform for Differentiating Background and Surface Interactions Using an Array of Metal-Insulator-Metal Resonators," IEEE Sens. J., vol. 16, no. 6, pp. 1621–1627, Mar. 2016.

[7] A. Mataji-Kojouri, M. O. Ozen, M. Shahabadi, F. Inci, and U. Demirci, "Entangled Nanoplasmonic Cavities for Estimating Thickness of Surface-Adsorbed Layers," ACS Nano, p. acsnano.0c02797, 2020.

[8] M. Shahabadi and K. Schunemann, "Millimeter-wave holographic power splitting/combining," IEEE Trans. Microwave Theory Tech., vol. 45, no. 12 PART 2, pp. 2316–2323, 1997.

[9] M. Rajibul Islam, M. Mahmood Ali, M. H. Lai, K. S. Lim, and H. Ahmad, "Chronology of Fabry-Perot Interferometer Fiber-Optic Sensors and Their Applications: A Review," Sensors, vol. 14, no. 4, pp. 7451–7488, Apr. 2014.

[10] P. J. De Groot, "A review of selected topics in interferometric optical metrology," Reports Prog. Phys., vol. 82, no. 5, p. 056101, Apr. 2019.

[11] K.-S. Isleif et al., "Experimental demonstration of deep frequency modulation interferometry," Opt. Express, Vol. 24, Issue 2, pp. 1676-1684, vol. 24, no. 2, pp. 1676–1684, Jan. 2016.

[12] G. Heinzel et al., "Deep phase modulation interferometry," Opt. Express, vol. 18, no. 18, pp. 19076–19086, Aug. 2010.

[13] O. Gerberding, "Deep frequency modulation interferometry," Opt. Express, vol. 23, no. 11, p. 14753, Jun. 2015.

[14] J. Zheng, "Optical frequency-modulated continuous-wave interferometers," Appl. Opt., vol. 45, no. 12, pp. 2723–2730, Apr. 2006.

[15] J. Zheng, Optical frequency-modulated continuous-wave (FMCW) interferometry. New York, NY, USA: Springer, 2005.

[16] M. Shahabadi, S. Atakaramians, and N. Hojjat, "Transmission line formulation for the full-wave analysis of two-dimensional dielectric photonic crystals," IEE Proc. Sci. Meas. Technol., vol. 151, no. 5, pp. 327–334, Sep. 2004.

[17] M. A. Boroujeni and M. Shahabadi, "Modal analysis of multilayer planar lossy anisotropic optical waveguides," J. Opt. A Pure Appl. Opt., vol. 8, no. 10, p. 856, Aug. 2006.

[18] M. A. Boroujeni and M. Shahabadi, "Full-wave analysis of lossy anisotropic optical waveguides using a transmission line approach based on a Fourier method," J. Opt. A Pure Appl. Opt., vol. 8, no. 12, p. 1080, Nov. 2006.

[19] M. Rajaei and M. Shahabadi, "Analysis of 2-D dielectric-waveguide-coupled optical ring resonators using a Transmission-Line Formulation," J. Opt. Soc. Am. A, vol. 32, no. 10, p. 1797, Oct. 2015.

[20] Z. Serahati, M. Rajaei, and M. Shahabadi, "Analysis of integrated MIM-based plasmonic devices using a Transmission-Line Formulation," J. Opt. Soc. Am. B, vol. 32, no. 9, p. 1843, Sep. 2015.

[21] H. Fadakar, A. Z. Nezhad, A. Borji, and M. Shahabadi, "Spurious-free analysis of two-dimensional low-loss metallic gratings," J. Opt. (United Kingdom), vol. 18, no. 3, Feb. 2016.

[22] S. Jalaly, M. Vahdani, M. Shahabadi, and G. M. Mohamad Sadeghi, "Design, fabrication, and measurement of a polymer-based anti-reflection coating for improved performance of a solar panel under a specific incident angle," Sol. Energy Mater. Sol. Cells, vol. 189, pp. 175–180, Jan. 2019.

[23] M. Vahdani, S. Yaraghi, H. Neshasteh, and M. Shahabadi, "Narrow-Band 4.3μm Plasmonic Schottky-Barrier Photodetector for CO2 Sensing," IEEE Sensors Lett., vol. 3, no. 3, pp. 1–4, Mar. 2019.

[24] R. Magnusson and S. S. Wang, "New principle for optical filters," Appl. Phys. Lett., vol. 61, no. 9, p. 1022, Jun. 1998.

[25] R. Magnusson, Y. Ding, K. J. Lee, P. S. Priambodo, and D. Wawro, "Characteristics of resonant leaky-mode biosensors," Proc. SPIE, vol. 6008, pp. 154–163, Nov. 2005.

[26] M. El Beheiry, O. Levi, S. Fan, and V. Liu, "Sensitivity enhancement in photonic crystal slab biosensors," Opt. Express, vol. 18, no. 22, pp. 22702–22714, Oct. 2010.

[27] A. G. Brolo, "Plasmonics for future biosensors," Nat. Photonics, vol. 6, no. 11, pp. 709–713, Nov. 2012.

[28] N. Nehru, E. U. Donev, G. M. Huda, L. Yu, Y. Wei, and J. T. Hastings, "Differentiating surface and bulk interactions using localized Surface Plasmon resonances of gold nanorods," Opt. Express, vol. 20, no. 7, p. 6905, Mar. 2012.

[29] N. Nehru, L. Yu, Y. Wei, and J. T. Hastings, "Using U-shaped localized Surface Plasmon resonance sensors to compensate for nonspecific interactions," IEEE Trans. Nanotechnol., vol. 13, no. 1, pp. 55–61, Jan. 2014.

[30] B. Zeng, Y. Gao, and F. J. Bartoli, "Differentiating surface and bulk interactions in nanoplasmonic interferometric sensor arrays," Nanoscale, vol. 7, no. 1, pp. 166–170, 2015.

[31] D. L. M. Rupert et al., "Dual-Wavelength Surface Plasmon Resonance for Determining the Size and Concentration of Sub-Populations of Extracellular Vesicles," Anal. Chem., vol. 88, no. 20, pp. 9980–9988, Oct. 2016.

[32] J. Juan-Colás, T. F. Krauss, and S. D. Johnson, "Real-Time Analysis of Molecular Conformation Using Silicon Electrophotonic Biosensors," ACS Photonics, vol. 4, no. 9, pp. 2320–2326, Sep. 2017.

[33] A. Abumazwed, W. Kubo, T. Tanaka, and A. G. Kirk, "Improved method for estimating adlayer thickness and bulk RI change for gold nanocrescent sensors," Sci. Rep., vol. 8, no. 1, Dec. 2018.

HOW TO CITE THIS ARTICLE

A. Mataji-Kojouri, A. Nooramin, M. Shahabadi, Optical Sensors for Industrial and Biomedical Applications. AUT J. Elec. Eng., 54(special issue 2) (2022) 333-342.

DOI: 10.22060/eej.2022.21376.5471